Scientific Papers of the University of Pardubice, Series A; Faculty of Chemical Technology
25 (2019) 75–82.

University of Pardubice
Faculty of Chemical Technology

The effect of calcination on the hydroxyapatite structure

Lenka Šimková* and Petra Šulcová

Department of Inorganic Technology,
The University of Pardubice, CZ–532 10 Pardubice, Czech Republic

Received: April 4, 2019; Accepted: May 5, 2019

The main objective of this work is the synthesis of hydroxyapatite powder with a general formula $Ca_{10}(PO_4)_6(OH)_2$ by the precipitation method with the following synthetic conditions: the Ca/P ratio = 1, the range of pH value = 7, where ammonia hydroxide solution was used to adjust the pH, and the rate of precipitation of ammonium dihydrogen phosphate was determined to 2 $ml \cdot min^{-1}$. Yet another aim of this paper was to characterize the physicochemical properties of the hydroxyapatite phase and subsequently to evaluate the effect of firing temperatures on the hydroxyapatite structure. The synthesized powder was characterized by X-ray diffraction (XRD) in order to identify the phase composition and crystallinity; the morphology of synthesized powder having been studied by scanning electron microscopy (SEM) and the prepared powder analyzed with respect to the particle size distribution (PSD).

Keywords: Hydroxyapatite; Precipitation; Calcination; PSD; XRD; SEM

Introduction

The term “apatite” applies to a group of compounds with a general formula $M_{10}(XO_4)_6Z_2$, where Z^- is typically OH^-, F^-, Cl^-. The cationic positions of M^{2+} can be completely or partially replaced by the Sr^{2+}, Ba^{2+}, Pb^{2+}, Na^+, etc. The apatite phosphate grid, XO_4^{3-}, is highly tolerant to substitution and can be replaced by the CO_3^{2-}, HPO_4^{2-}, AsO_4^{3-}, SiO_4^{2-}, or VO_4^{3-} groups [1]. Hydroxyapatite (HAP) has the molecular structure of apatite, where M is calcium (as Ca^{2+}), X is phosphorus (P^{5+}) and Z is the hydroxyl group (OH^-). The chemical formula of HAP is $Ca_{10}(PO_4)_6(OH)_2$, with 39.89 % by weight of calcium, 18.50 % of phosphorus, 41.41 % of oxygen, and 0.20 % of hydrogen [2,3].

* Corresponding author, ✉ lenka.simkova1@student.upce.cz

The relevant consideration is paid to the use of hydroxyapatite, especially in the field of orthopedics, where these phosphates can replace partially or totally the bone tissue [4,5]. With respect to hydroxyapatite (HAP), it is an important technological material, whose applications include its use on metal implants as a coating which has two important functions: to protect the implant against corrosion and to improve implant's biocompatibility with the human body [2,6]. Since the HAP is convenient for the protection of the implants against corrosion for its structural and physicochemical properties, it can be expedient as a corrosion inhibitor like the other phosphates [4].

Hydroxyapatite can be produced synthetically by using a number of different methods, such as reactions in solid state [7], coprecipitation [8,9], hydrothermal methods [10], the sol-gel process [11,12], microwave processing [13], or even other [14]. The most common approaches are chemical coprecipitation from water solutions, under precipitation conditions of pH ~ 7, when primary crystallites of insoluble hydroxyapatite are formed [14]. In the coprecipitation method, there are two types of process: one involving the reaction of calcium and phosphate salts (described in this paper)

$$10\ Ca(NO_3)_2{\cdot}4H_2O + 6\ (NH_4)H_2PO_4 + 8\ NH_4OH \rightarrow Ca_{10}(PO_4)_6(OH)_2 + 20\ NH_4NO_3 + 46\ H_2O$$

and, the other representing the neutral reaction of an acid with alkaline solutions [15].

In the previous study [16], the effect of precipitation conditions on hydroxyapatite synthesis and structure has already been demonstrated. Based on these results, the following synthesis conditions were selected for the research: Ca/P = 1, pH = 7 and precipitation rate = 2 $ml \cdot min^{-1}$. The work presented herein is focused on the synthesis of hydroxyapatite by the precipitation method and subsequent firing temperatures of the prepared samples. Synthesized pigments were evaluated in terms of the particle size distribution, crystal size, and morphology, as well as via phase composition.

Materials and methods

Synthesis of hydroxyapatite powder

Hydroxyapatite $Ca_{10}(PO_4)_6(OH)_2$ was synthesized by precipitation method using the following starting compounds: $Ca(NO_3)_2{\cdot}4H_2O$ (98 %, Lachema, Brno, Czech Republic), $(NH_4)H_2PO_4$ (98 %, Lachema, Brno, Czech Republic), NH_4OH (25 %, Penta, Chrudim, Czech Republic). The precise concentrations of starting solutions were determined using the respective analytical methods [16,17].

The sample was prepared by precipitation of starting compounds $Ca(NO_3)_2$ and $NH_4H_2PO_4$, where NH_4OH was used to adjust the pH. This was followed by the aging of the prepared sample for 24 hours. After such an aging, the particle

size analysis was performed (PSD, Mastersizer 2000/MU, Malvern Instruments, Worcestershire, UK) followed by filtration (with Büchner system), washing and drying (80 °C for 6 hours) of the sample. The next analysis was performed using scanning electron microscopy (SEM LYRA 3, Tescan, Brno, Czech Republic) and X-ray diffraction (XRD MiniFlex 600, Rigaku, Tokyo, Japan).

Characterization of hydroxyapatite

The synthesized powder was characterized in order to identify the phase composition and crystallinity (XRD), for the morphology (SEM) and particle size distribution (PSD).

The particle size distribution of the synthesized powder was measured using an equipment Mastersizer 2000/MU. This device provides an option to perform volumetric distribution and uses the laser diffraction on particles dispersed in a liquid medium. The particle size distribution was analyzed by two lasers: blue light (laser diode with wavelength of 466 nm) and red light (He–Ne laser with wavelength of 633 nm). The pigment was ultrasonically homogenized (Bandelin, Berlin, Germany) in the solution of $Na_4P_2O_7$ (c = 0.15 mol dm^{-3}) for 30 min. The signal was evaluated on the basis of Mie scattering. The measurement was taken in three steps, and results automatically calculated as average and presented as the d_{10}, d_{50}, and d_{90} values.

The phase analysis of the powdered material was studied by X-ray diffraction analysis (XRD). The phase composition was determined using diffractometer MiniFlex 600 equipped with a vertical goniometer of 17 cm in the 2θ range of 10–50°. The accuracy of goniometer was ±0.02°, when X-ray tube with Cu anode (U = 40 kV, I = 15 mA) was used (CuKα radiation).

The morphology of the prepared powder was determined using a scanning electron microscope (SEM) equipped with EDS analyzer AZtec X-Max 20 (Oxford Instruments, Concord, MA, USA) at an acceleration voltage of 20 kV. The resulting image was formed by the secondary signal – reflected or secondary electrons.

Results and discussion

Particle size distribution analysis

Particle size distribution of the prepared sample was measured after one-day aging with the equipment Mastersizer 2000/MU. Signal was assessed by Mie scattering theory. The distribution curves and d_{10}, d_{50}, d_{90} and distribution span were gained. Fig. 1 demonstrates the distribution curves of hydroxyapatite (HAP 1), which has been subjected to firing temperature at 800, 1000, 1100 and 1200 °C. The width of the distribution ranges from 0.3 to 400 μm in the particle size range. Table 1

introduces the particle size values d_{10}, d_{50}, d_{90} and the distribution span of the measured samples. For the samples measured, the d_{10} value is in the range from 0.77 to 3.52 µm, the d_{50} value lies from 5.93 to 13.24 µm, the d_{90} value is from 22.43 to 72.93 µm. The distribution of all samples analyzed spans from 2.27 to 5.60.

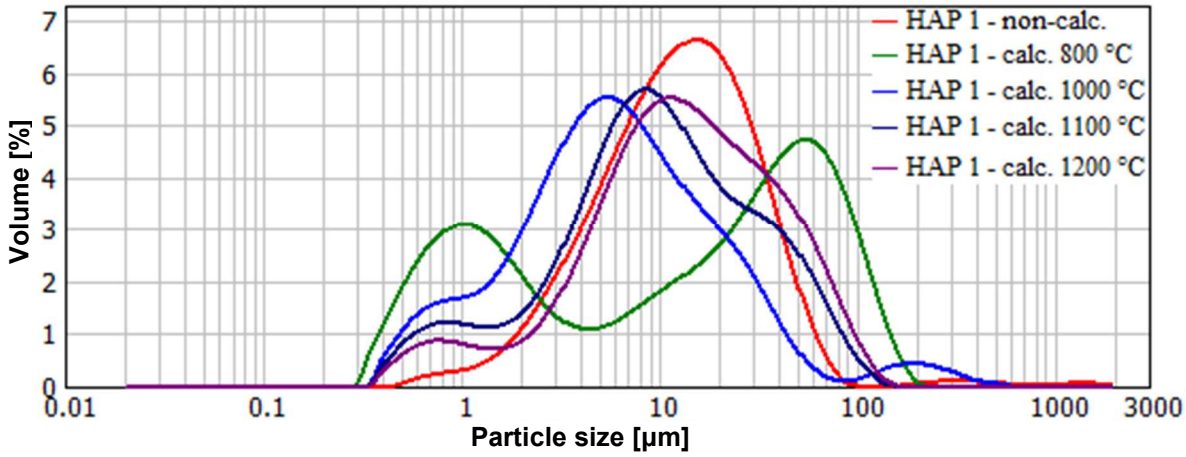

Fig. 1 Distribution curves of all synthesized samples

Table 1 Particle size distribution of prepared samples

t [°C]	d_{10} [µm]	d_{50} [µm]	d_{90} [µm]	span
800	0.77	12.88	72.93	5.60
1000	1.19	5.93	27.59	4.46
1100	1.70	9.66	43.95	4.38
1200	2.75	13.24	52.25	3.74
Non-calc.	3.52	9.80	22.43	2.27

From the particle size distribution (Table 1), it is evident that growing firing temperature causes an increase of the value of d_{50} (for temperatures 1000 °C and higher) and conversely decreases the value of span. For the firing temperature of 800 °C, the higher value of d_{50} was achieved, which may be attributed to the presence of a larger proportion of small particles in the volume and the occurrence of agglomerates of larger particles, caused to the short dispersion time in the ultrasonic bath. The width of particle size distribution is in the range of 0.3 to 400 µm, which is obvious from the graph (see again Fig. 1). From the width of particle size distribution, it can be concluded that the use of higher firing temperature, the number of small particles in the volume decreases. Subsequently, the formation of agglomerates of larger particles occurs, which is prove in the width of the distribution curve, which moves towards higher values.

X-ray diffraction analysis

The phase composition of the samples was determined by XRD analysis. A hexagonal structure of hydroxyapatite was identified. Fig. 2 shows the diffractogram of samples 1 containing the hydroxyapatite diffraction line $Ca_{10}(PO_4)_6(OH)_2$ (“**∇**”, HAP 1– Non-calc.) with the parameters: hexagonal crystalline system; space group $P6_3/m$. Fig. 2 also illustrates the diffractogram of fired samples containing the tricalcium phosphate diffraction line β-$Ca_3(PO_4)_2$ (“*****”, TCP) with the following parameters:

- 800, 1000 and 1100 °C: trigonal crystalline system; space group R–3c;
- 1200 °C: trigonal crystalline system, space group R-3c and for α-$Ca_3(PO_4)_2$ (“•”): orthorhombic crystalline system.

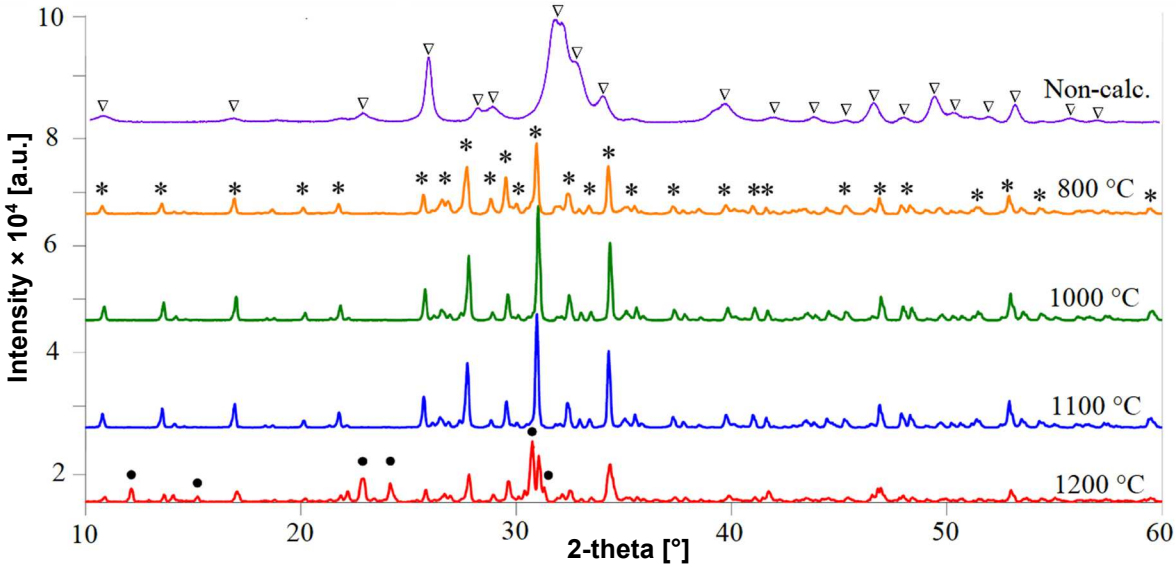

Fig. 2 X-ray diffraction patterns of hydroxyapatite samples
(∇ = $Ca_{10}(PO_4)_6(OH)_2$; * = β-$Ca_3(PO_4)_2$; • = α-$Ca_3(PO_4)_2$)

From the diffractogram (Fig. 2), it is clear that during the firing process the phase change occurs, which leads to the formation of TCP (tricalcium phosphate; $Ca_3(PO_4)_2$) as the main product of the decomposition of HAP. From these results, it is obvious that the during of firing process occurs of HAP transformation into its main degradation product (β-TCP), converting into the “α” modification at higher firing temperatures (1200 °C).

Scanning electron microscope

Measurement by SEM was performed after sample drying. The measured samples proved the effect of different firing temperatures on the sample morphology (Figs. 3 and 4).

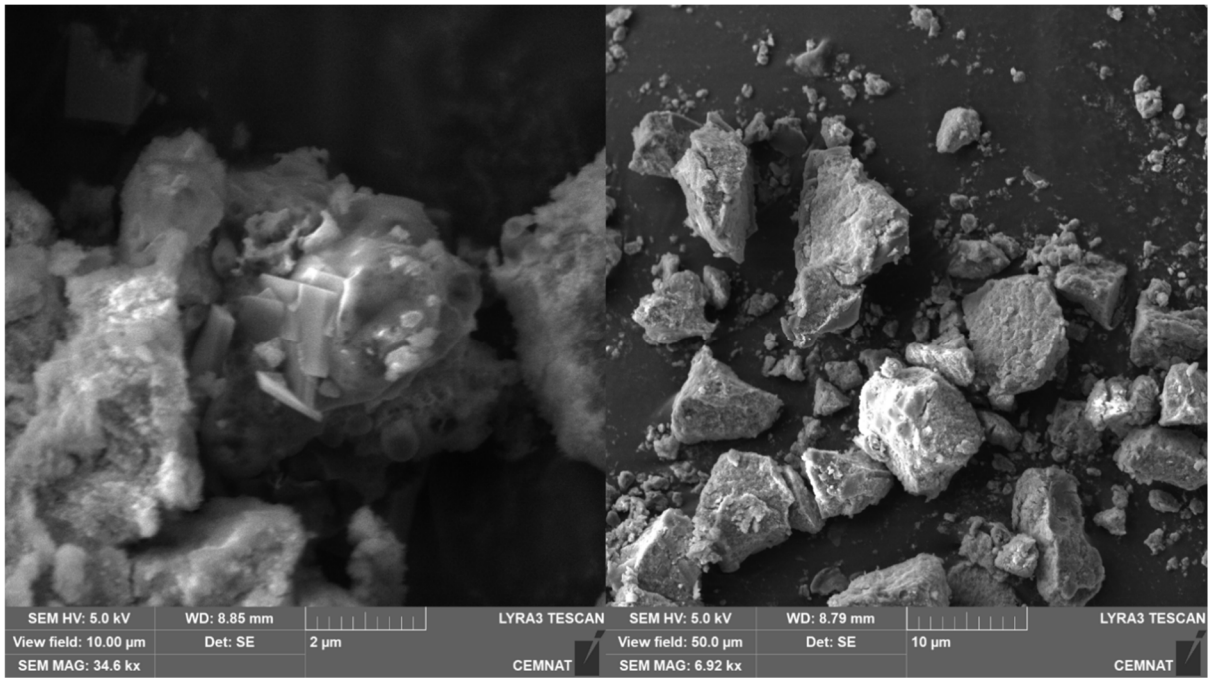

Fig. 3 SEM images of sample HAP 1 before calcination

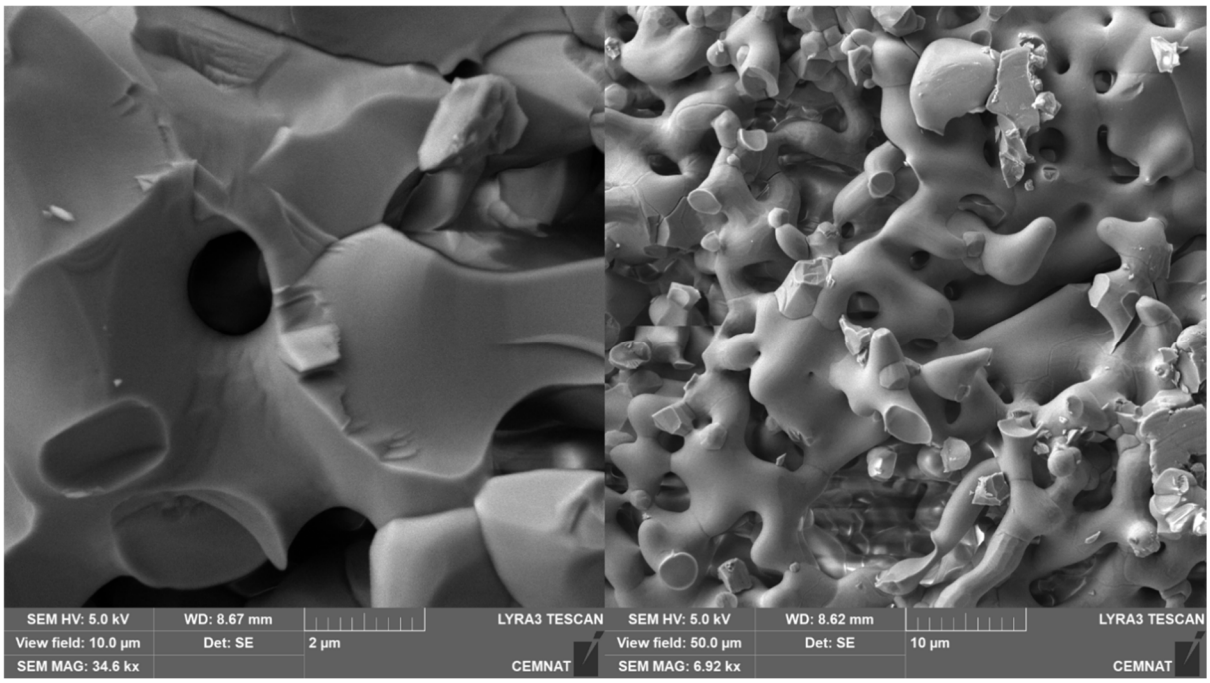

Fig. 4 SEM images of sample HAP 1 after calcination at 1200 °C

From the SEM scans, it is distinct that both sintering and crosslinking of molecules occur during the firing process.

Conclusion

The selected synthesis conditions are suitable for the formation of crystalline hydroxyapatite phase. From the performed analyses, it is obvious that the firing temperature has had significant impact on the structure and morphology of hydroxyapatite.

From the particle size distribution analysis, it is evident that growing firing temperature causes an increasing of the values of d_{50} (except for firing temperature of 800 °C), and vice versa, decreasing the values of the span. From the width of particle size distribution it follows that the use of higher firing temperature decreases the number of small particles in the volume.

By the XRD analysis, it is clear that during the firing process the phase change occurs, which leads to the formation of TCP. A next step, during the firing process, is the transformation of HAP into its main degradation product (β-TCP), which is further converted into the "α" modification at higher firing temperatures (1200 °C).

Finally, based on the SEM images, it is apparent that sintering and crosslinking of molecules take place during the firing process.

Acknowledgments

This work has been supported by University of Pardubice under the project SGS_2019_004. The authors appreciate a financial support from LM2015082 granted by the Ministry of Education, Youth and Sports of the Czech Republic and European Regional Development Fund-Project "Modernization and upgrade of the CEMNAT" (No. CZ.02.1.01/0.0/0.0/16_013/0001829).

References

[1] Elliott J.C.: *Structure and chemistry of the apatites and other calcium orthophosphates*. Elsevier Science, London 1994.

[2] Rivera-Muñoz E.M.: *Hydroxyapatite – based materials: synthesis and characterization*. IntechOpen, London 2011.

[3] Friedman H.: *Complete information guide to rock, minerals and gemstones: The apatite mineral group.* https://www.minerals.net (accessed February 10, 2019).

[4] Gorodylova N., Dohnalová Ž., Šulcová P., Bělina P., Vlček M.: Influence of synthesis conditions on physicochemical parameters and corrosion inhibiting aktivity of strontium pyrophosphates $SrM^{II}P_2O_7$ (M^{II} = Mg and Zn). *Progress in organic coating* **93** (2016) 77–86.

[5] Kalenda P., Veselý D., Antoš P.: *Corrosion and anticorrosion protection of metallic materials* (in Czech). Univerzita Pardubice, Pardubice 2003.

[6] Huang Y., Hao M., Nian X., Qiao H., Zhang X., Zhang X., Song G., Guo J., Pang X., Zhang H.: Strontium and copper co-substituted hydroxyapatite-based coatings with improved antibacterial activity and cytocompatibility fabricated by electrodeposition. *Ceramics International* **42** (2016) 11876–11888.

[7] Arita I.H., Castano V.M., Wilkinson D.S.: Synthesis and processing of hydroxyapatite ceramic tapes with controlled porosity. *Journal of Materials Science* **6** (1995) 19–23.

[8] Akao M., Aoki H., Kato K.: Mechanical properties of sintered hydroxyapatie for prothetic applications. *Journal of Materials Science* **16** (1981) 809–812.

[9] Kong LB., Ma J., Boey F.: Nanosized hydroxyapatite powders derived from coprecipitation process. *Journal of Materials Science* **37** (2002) 1131–1134.

[10] Zhang X., Vecchio K.S.: Hydrothermal Synthesis of Hydroxyapatite Rods. *Journal of Crystal Growth* **308** (2007) 133–140.

[11] Wang J., Shaw L.L.: Synthesis of high purity hydroxyapatite nanopowder via sol–gel combustion process. *Journal of Materials Science* **20** (2009) 1223–1227.

[12] Jillavenkatesa A.: Sol–gel processing of hydroxyapatite. *Journal of materials science* **33** (1998) 4111– 4119.

[13] Yang Y., Ong J.L., Tian J.: Rapid sintering of hydroxyapatite by microwave processing. *Journal of Materials Science Letters* **21** (2002) 67– 69.

[14] Safronova T.V., Shekhirev M.A., Putlyaev V.I.: Ceramics Based on Calcium Hydroxyapatite Synthesized in the Presence of PVA. *Glass and Ceramics* **64** (2007) 408–412.

[15] Vazquez C.G., Barba C.P., Munguia N.: Stoichiometric hydroxyapatite obtained by precipitation and sol gel processes. *Revista Mexicana de Fisica* **51** (2005) 284–293.

[16] Šimková L., Gorodylova N., Dohnalová Ž., Šulcová P.: Influence of precipitation conditions on the synthesis of hydroxyapatite. *Ceramics and Silikáty* **62** (2018) 253–260.

[17] Přibil R.: *Complexometry* (in Czech). SNTL, Prague 1961.